

Strain-Induced Martensitic Transformation and the Mechanism of Wear and Rolling Contact Fatigue of AISI 301LN Metastable Austenitic Stainless Steel

Tshenolo P. Leso,* Tulani W. Mukarati, Roelf J. Mostert, and Charles W. Siyasiya

AISI 301LN metastable austenitic stainless steels (MASSs) are known to exhibit high work-hardening rates attributed to martensite evolution during straining which results in the second-phase strengthening mechanism. This enhances surface hardness and potentially reduces wear and rolling contact fatigue (RCF). The aim of this study is therefore to evaluate the work hardening, wear, and RCF performance of AISI 301LN metastable austenitic stainless steel as a possible alternative material for rolling and sliding applications by varying the contact conditions such as slip ratio against the standard R350HT rail steel using a twin-disc simulator. The results show that 301LN MASS has high surface work hardening and increased hardness because of martensitic transformation, while R350HT rail steel has only slightly changed. The formation of a hard martensitic phase is also confirmed by X-ray diffraction analysis as well as by two other techniques, indicating a secondary hardening effect. Although it shows potential for work hardening, its susceptibility to wear-related problems may make it less suitable for rolling and sliding applications due to a cracking and spalling mechanism induced by martensite formation. The surface strains required for the observed martensite formation are calculated and found to be very high, approaching 0.4.

1. Introduction

This work intends to explore the possibility of using metastable austenitic stainless steels (MASSs) for the manufacturing of sliding and rolling components such as train wheels, gears, etc. due to their high strain-hardening capabilities. MASS is


predominantly purely austenitic at room temperature; however, the austenite phase is not thermodynamically stable. The austenite phase can transform to martensite as a result of plastic deformation at temperatures lower than the M_d temperature which is known as strain-induced martensitic transformation. The austenite phase is softer than the strain-induced martensite phase and the martensite formation during cold working increases the material hardness significantly.^[1] Traditionally, these types of steels have applications in crash-worthiness in the automotive industry, for crash—relevant parts of bodywork casing due to their extremely high strain—hardening capacity.^[2,3] Although the extremely high strain-hardening capacity has obvious advantages as far as wear resistance is concerned, there is no work reported in the literature where MASS has been applied in rolling and sliding applications. In railway applications, it is well known that the hardness of the wheels and rail should be related to minimize the

wear and rolling contact fatigue (RCF), i.e., with a wheel-to-rail hardness ratio of close to 1 (hardness ratio is equal to wheel hardness divided by rail hardness).^[4] Although the pure austenitic phase in MASS is softer than pearlitic R30HT rail steel, it has been hypothesized that as a result of rolling and sliding contact under application of load, surface martensitic transformation will take place leading to increase in hardness until it matches the hardness of the rail, then afterward, the wear loss of the wheels should be consistently low.

The high cost of such alloys can potentially be offset by the increased wear life of the wheel and/ or by selective application of the alloy to the wheel surface by means of a sleeve or similar. The superior corrosion resistance of the MASSs is thought to have obvious benefits as far as corrosion-wear performance is concerned. It is known that martensitic transformation is accompanied by some volume change depending on the alloy composition,^[5–7] and the dimensional tolerance should be considered within the design of such wheels. Other potential advantages of using MASSs as train wheels are the in situ, non-destructive, and easy monitoring of martensite content during the inspection using simple equipment such as Ferritescope which measures the volume fraction of only the magnetic phase, in which case it will be martensite as the austenite phase is

T. P. Leso, T. W. Mukarati, R. J. Mostert, C. W. Siyasiya
Department of Materials Science and Metallurgical Engineering
University of Pretoria
Lynnwood Road, Hatfield 0083, South Africa
E-mail: u19345314@tuks.co.za

T. P. Leso
Department of Chemical, Materials and Metallurgical Engineering
Botswana International University of Science and Technology
Palapye, Botswana

 The ORCID identification number(s) for the author(s) of this article can be found under <https://doi.org/10.1002/srin.202400128>.

© 2024 The Author(s). Steel Research International published by Wiley-VCH GmbH. This is an open access article under the terms of the Creative Commons Attribution License, which permits use, distribution and reproduction in any medium, provided the original work is properly cited.

DOI: 10.1002/srin.202400128

nonmagnetic. The accumulated surface strain damage of the wheel could be easily tracked by the in situ martensitic measurements. Thorough cost–benefit analysis of using MASSs as an alternative material for train wheels would have to be done if they are to replace bainitic or pearlitic steels, which necessitates quantification of the relative wear performance of such alloys. During rolling and sliding of MASSs under static load, the material experiences some deformation thereby increasing the contact temperature due to frictional heat generated at the contact area. The deformation experienced during contact results in some transformation of austenite to martensite. The transformation is temperature dependent, with an increase in the deformation temperature resulting in a decrease in the driving force to induce martensitic transformation.^[1,8,9] As part of this work, the effect of slip ratio was investigated at the contact. Changing the slip ratio has been found to have an effect on the contact temperature with contact temperature increasing with the slip ratio as previously discussed in literature.^[10] This effect of slip ratio on contact temperature was studied to find out how it affects the austenite to martensite transformation during rolling and sliding simulation and thereby the wear rate. Previous works^[11–13] on SAE 4320 and SAE 52100 steels, respectively, have shown that, for conventional alloy steels, austenite does transform to deformation-induced martensite under rolling and sliding contact.^[14]

This study focuses on the possible advantages of employing AISI 301LN MASS for railway wheels, considering its prolonged service life and enhanced performance attributes. AISI 301LN stainless steel could offer long-term cost savings through reduced replacements and maintenance interventions, alongside improved mechanical properties leading to enhanced performance and reliability. Additionally, it is also a good option for train wheels because of its great strength and resistance to corrosion, which could eventually lessen wear and RCF. Moreover, the study might drive advancements in materials science and engineering, which could result in the creation of customized production techniques and their extensive implementation in the railway sector. In future, it is crucial to determine whether MASSs are a feasible substitute for conventional wheel steels, a comprehensive wear performance assessment and a cost-benefit analysis will be necessary which was not part of this study.

2. Experimental Section

2.1. Material Preparation

R350HT rail steel^[15] was used for rail discs while AISI 301LN metastable austenitic stainless steel was used to manufacture wheel discs. The rail has an as-received hardness of 407 ± 5 HV10 while for AISI 301LN, it was 254 ± 5 HV10, obtained using Struers Duramin-40 hardness tester under a load of 10 kgf. The chemical composition for the R350HT rail steel

and AISI 301LN MASS are shown in **Table 1** obtained using optical emission spectrometry. For the as-received microstructures, the R350HT rail was ground and polished to 1 μm surface finish and then etched with Nital etchant (2%) whereas the AISI 301LN steel was electropolished by Struers A3 solution and etched using aqua regia which is a 3:1 mixture of hydrochloric acid and nitric acid, respectively. Optical microscopy (OM) and scanning electron microscopy (SEM) were used to obtain the as-received microstructures, as shown in **Figure 1**. Rail discs were sectioned from the rail head as discussed in the literature^[16–18] ensuring that there are homogenous radial microstructures and mechanical properties.

2.2. Wear Testing and Simulation

For wear testing, a University of Pretoria developed twin-disc rig (**Figure 2**)^[19] was used which uses the principle of two rotating discs rotating at opposite angular speeds under a contact load. The details of its operation have been described in previous work.^[19] The twin disc test approach consists of two rotating discs (cylinders) made of wheel and rail steel specimens to simulate the wheel/rail contact. This concept is easier to control and incorporates comprehensive data collection capabilities.^[20] It offers the ability to control the slip ratio between the contacting discs by rotating them at different speeds simulating the movement of the wheel along the rail.^[21] Literature^[22,23] has demonstrated that slip ratio varies at the wheel–rail contact as the wheel moves along the track whether at steady speeds, under acceleration, or breaking. From the results, wear rates can be obtained to model the wear regimes being mild, severe, and catastrophic as described in literature.^[16,24,25] Other test approaches include pin-on-disc; block-on-ring; pin-on-reciprocating plate; twin disc; and ring-on-ring which were not used for this work due to their limitation in simulating rolling and sliding wear as the wheel moves along the rail.

The discs had a diameter of 50 mm and width of 5.5 mm, loaded in a vertical configuration as shown in **Figure 3**. Tests were conducted at four slip ratios, 2, 5, 10, and 20% under a contact load of 1.4 kN corresponding to 860 MPa contact pressure using Hertz theory.^[26,27] The R350HT rail disc was set to be the braking disc with a constant speed of 340 rpm while the AISI 301LN disc was the driving disc and its speed was set to achieve the four slip ratios. To calculate slip ratios, Equation (1) was used, where V_w and V_r are the angular velocities of wheel and rail discs in revolutions per minute (rpm), and R_w and R_r are the rolling radii of the wheel and rail discs, respectively.^[19] In this investigation, the radii of both the wheel and rail discs are identical. From measured torque values, friction coefficient values were calculated using Equation (2), where T is torque (Nm), and F is the contact load (N):

$$\text{Slip ratio} = \left(\frac{V_w \times R_w - V_r \times R_r}{V_w \times R_w + V_r \times R_r} \right) \times 200\% \quad (1)$$

Table 1. Chemical composition of the MASS wheel (AISI 301LN) and the popular rail steel (R350HT) with Fe as balance, wt%.

Element	C	Mn	S	P	Si	Ni	Cr	Mo	Cu	N	Fe
R350HT Rail	0.84	1.24	0.018	0.020	0.49	0.04	0.22	≤0.01	0.03	–	Balance
AISI 301LN	0.024	1.44	≤0.005	0.019	0.42	6.45	17.4	0.04	0.07	0.105	Balance

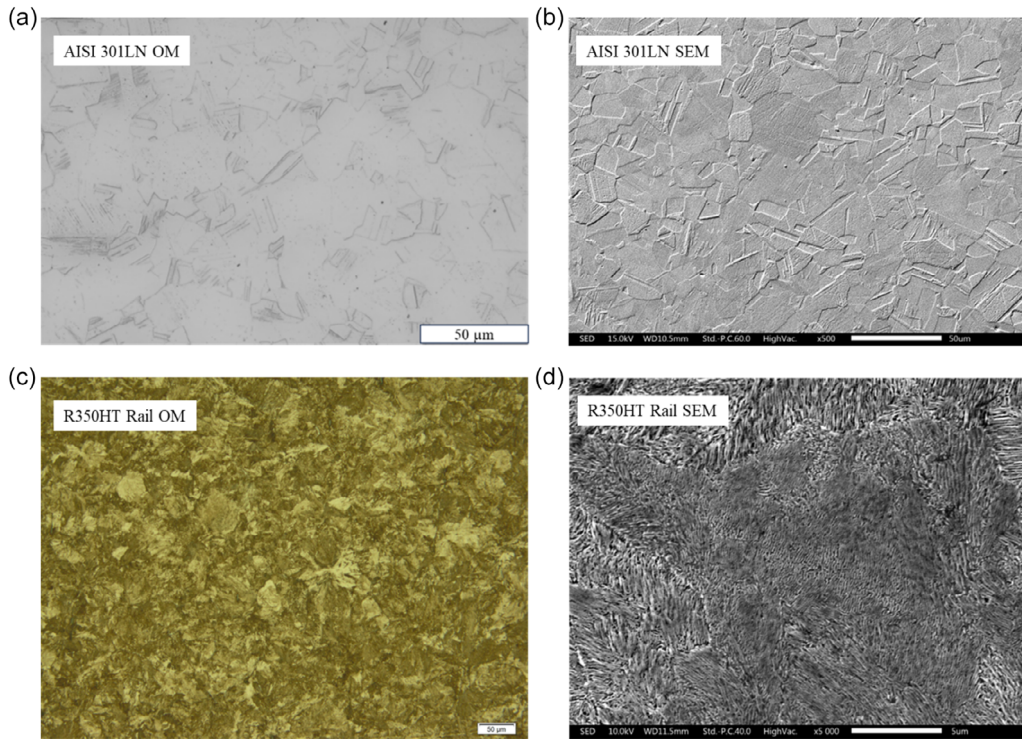


Figure 1. As-received micrographs of AISI 301LN stainless a) OM and b) SEM showing purely austenitic microstructures; as-received micrographs of R350HT rail c) OM and d) SEM showing pearlitic microstructure.

$$\mu = \frac{T}{FR_r} \quad (2)$$

All tests were conducted in a dry environment. To measure the 301LN disc temperature, during testing an infrared temperature sensor connected to CalexConfig data logging software was used. The temperature sensor had an accuracy of ± 1 °C, response time of 125 ms, and a measuring range of 300 mm hence high accuracy and precision. Before each test, all discs were washed in an ultrasonic bath of ethanol to remove any contamination and weighed. A Ferritescope (Helmut Fisher GmbH, model MP3B) was used to measure the amount of induced martensite (%) throughout the test after every 3400 rolling cycles at the contact surface of the AISI 301LN specimen. Ferritescope measurements served as a quick and nondestructive method for conducting in situ assessments of magnetic strain-induced martensite content throughout interrupted rolling cycles. Its operation principle is based on measuring the magnetic permeability of the material. However, the difference in measured amounts of martensite fractions arises due to the differing magnetic permeability of martensite compared to delta ferrite as Ferritescope device is made to measure the amount of delta ferrite in the austenitic stainless-steel weld metal. Therefore, it is important to make an adjustment or calibrate the readings when used for martensite fraction determination. From previous works on the same material by Mukarati et al.^[1,9] a calibration factor of 1.7 was used to convert Ferritescope measurements into the actual percentage of strain-induced martensite as per Equation (3) which was also adopted for this work. The calibration factor was determined

by comparing the values obtained from vibrating sample magnetization measurements, X-ray analysis, and neutron diffraction analyses with the readings from the Ferritescope. No thickness correction was necessary for Ferritescope measurements, as the sample thickness consistently exceeded 2 mm. The calibration factor of 1.7 was also found to be similar to the one determined in the study by Talonen et al.^[28] on similar material.

$$\text{Strain – induced martensite} = 1.7 \times \text{Ferritescope reading} \quad (3)$$

During Ferritescope measurements, a minimum of seven readings were taken at various points on the rolling disc's surface, with the probe oriented perpendicular to the sample surface. Mean and standard deviations were subsequently calculated. When measuring the amount of induced martensite (%) the test was stopped for a few seconds to minimize any temperature loss on the 301LN disc. At the end of the first test run (run 1), the discs were removed from the test rig washed in an ultrasonic bath of ethanol to remove any contamination and debris that formed during testing, and weighed to obtain mass loss. The same discs were rerun under test run 2 repeating the same procedure as test run 1 where a Ferritescope was used to measure the amount of induced martensite (%) throughout the test after every 3400 rolling cycles at the contact surface of the AISI 301LN specimen. The same was done across all the slip ratios. After test run 2, the discs were also washed in an ultrasonic bath of ethanol and weighed to obtain mass loss. The mass losses were used to calculate the wear rate. The wear rate ($\mu\text{g}/\text{m}/\text{mm}^2$) has been described by literature^[16,24,25] as the weight of lost material

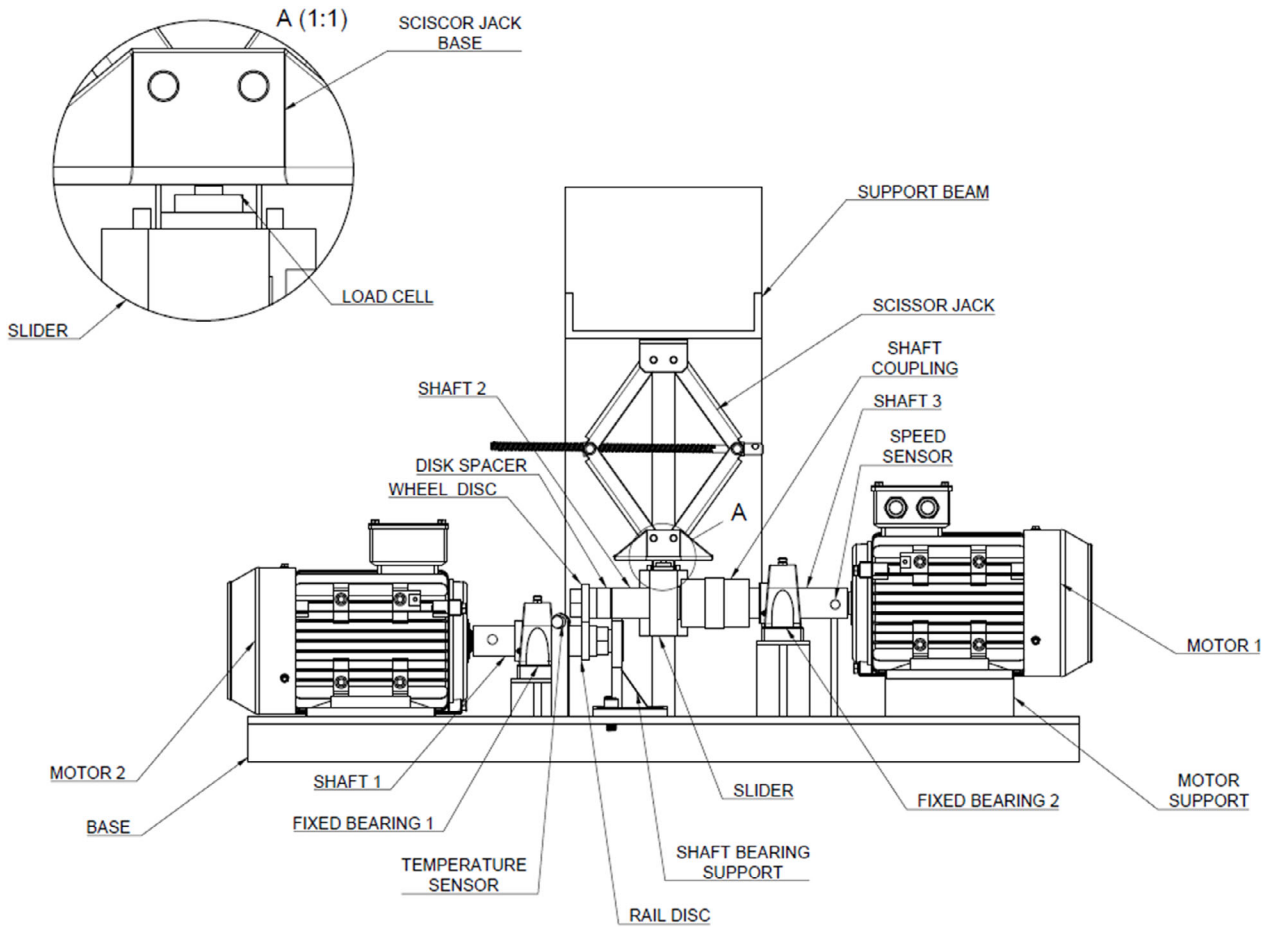


Figure 2. Schematic of the twin disc wear simulator.

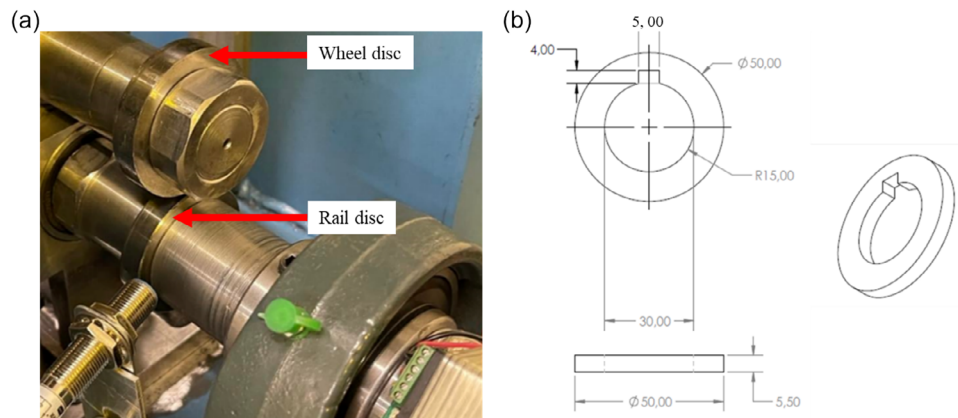


Figure 3. a) Test configuration showing the contact between the wheel and rail discs (vertical load configuration) and b) dimensions (mm) of AISI 301LN and R350HT rail discs specimens.

(μg) after test, per the traveled distance (m), per the area of contact between the discs (mm^2).

After test run 2, the worn discs were then observed under a microscope to obtain the morphology of the worn surfaces. Worn discs were sectioned in their cross-section and electropolished

(voltage 1.5 V time 20 s) for electron backscatter diffraction (EBSD) observation as well as to be examined using optical and scanning electron microscopies to observe any subsurface damage that might have occurred as well as to obtain the EBSD micrographs. Vickers microhardness profiles were

performed using Struers Duramin-40 hardness tester with a force of 300 gf along the three lines. The measurements were done from the contact surface toward the center with a spacing of 200 μm between the indents along the lines and 500 μm between the lines to a depth of 3.8 mm. The total area analyzed is 1×3.8 mm. X-ray diffraction (XRD) analysis was performed on the sectioned worn specimen sectioned using electrical discharge machining at the contact surface, at 1 and 2 mm depths using the PANalytical X'Pert Pro powder diffractometer in θ - θ configuration with an X'Celerator detector and variable divergence- and fixed-receiving slits with Fe filtered $\text{Co-K}\alpha$ radiation ($\lambda = 1.789 \text{ \AA}$). The resulting patterns were processed using HighScore Plus analytical software and the PanICSD database to identify all phases present (austenite and strain-induced martensite). The samples were prepared according to the standardized Panalytical backloading system, which provides a nearly random distribution of the particles.

3. Results and Discussion

3.1. Martensite Formation and Work Hardening Ability

During testing on the first run, the amount of strain-induced martensite increased significantly across all slip ratios up until 20 000 rolling cycles where the saturation point was reached and no further increase in martensite was observed, **Figure 4**. After the first run, the discs were removed from the rig and cleaned in an ultrasonic bath of ethanol then observed under OM and weighed for mass loss. For the second run, the same discs for each slip ratio were used, using the same procedure for measuring the amount of strain-induced martensite as test run 1 and there was not any change in the amount of strain-induced martensite, as observed in Figure 4, as the saturation has already been reached in test run 1. The amount of

strain-induced martensite increased with a decrease in slip ratio with 2% slip ratio showing the highest saturation point. The reason for this is due to contact temperature, at lower slip ratio the contact temperature is low (**Figure 5**), whereas increasing the slip ratio results in an increase in contact temperature, due to increased friction. At 2% slip ratio, the saturation martensite volume fraction was $48 \pm 2\%$ at the contact surface with a maximum contact surface temperature of 33 $^{\circ}\text{C}$, whereas when the slip ratio was increased to 20%, the saturation martensite volume fraction decreased to $30 \pm 3\%$ while the contact temperature increased to 83 $^{\circ}\text{C}$. In MASS, temperature plays a significant role in martensite formation as previously demonstrated in literature.^[1,29] An increase in the contact temperature with an increase in slip ratio results in a decrease in the driving force for the transformation of austenite to martensite, hence less martensite formation at high slip ratios is expected.

Figure 6 shows the microhardness profiles of the AISI 301LN steel at 2% and 20% slip ratios used to determine the depth of deformation as well as the work hardening response plotted using OriginLab software, determined at the end of the second run. At a higher slip ratio of 20% more plastic surface deformation due to twinning was observed as the AISI 301LN had higher percentage increase in hardness (58% increase) toward the surface, with a hardness of 400 HV0.3 observed close to the contact surface compared to the as-received hardness of 254 HV0.3. At 2% slip ratio the maximum hardness was recorded toward the surface as 369 HV0.3 which is a 45% increase in hardness. This is so because at higher slip ratio the rate of deformation is higher due to an increase in creep and frictional forces resulting in more twinning and higher dislocation density, hence a higher rate of work hardening occurred, increasing the material hardness and depth of deformation. Two localized regions of superior internal hardening, one at ≈ 1 mm depth and another at 1.5–2.0 mm depth, were also observed for the 20% slip ratio case. Generally, the subsurface hardening was observed to not be

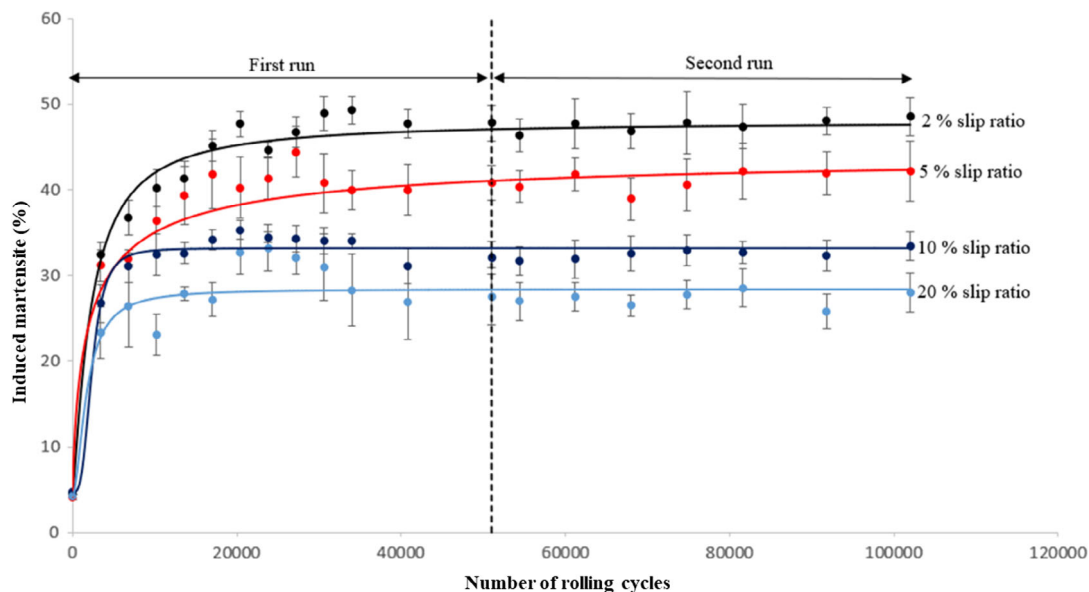


Figure 4. Induced martensite volume fraction (%) at the contact surface versus number of rolling cycles at different slip ratios obtained using Ferritescope readings.

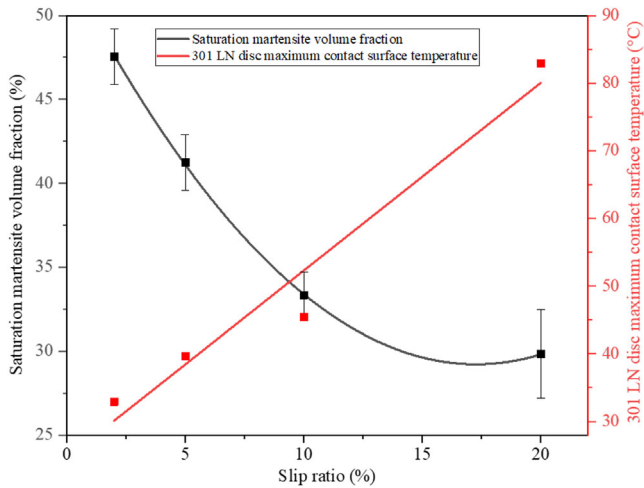


Figure 5. Saturation martensite volume fraction (%) at the contact surface and the 301 disc maximum contact surface temperature versus slip ratio.

a homogenous function of depth below the surface, probably as a consequence of the influence of shear deformation. For the R350HT rail, little to no work hardening was observed as there was no significant increase in hardness as compared to AISI 301LN steel. This is so because the rail had a higher as-received hardness value compared to the AISI 301LN steel and has an eutectoid microstructure which is not amenable to significant work hardening.

Figure 7 shows EBSD micrographs of 301LN specimen subjected to 2% and 20% slip confirming the presence of strain-induced martensite close to the contact surface, demonstrating that the wear test rig was successful in inducing martensite under rolling and sliding contact. To further confirm plastic deformation, inverse pole figure (IPF) maps were used with their corresponding misorientation plots, **Figure 8**. As may be seen, both the grain rotation and low-angle misorientation increased with an increase in the slip ratio due to increased plastic deformation. Higher slip ratios result in increased temperature due to adiabatic heating, which leads to deformation

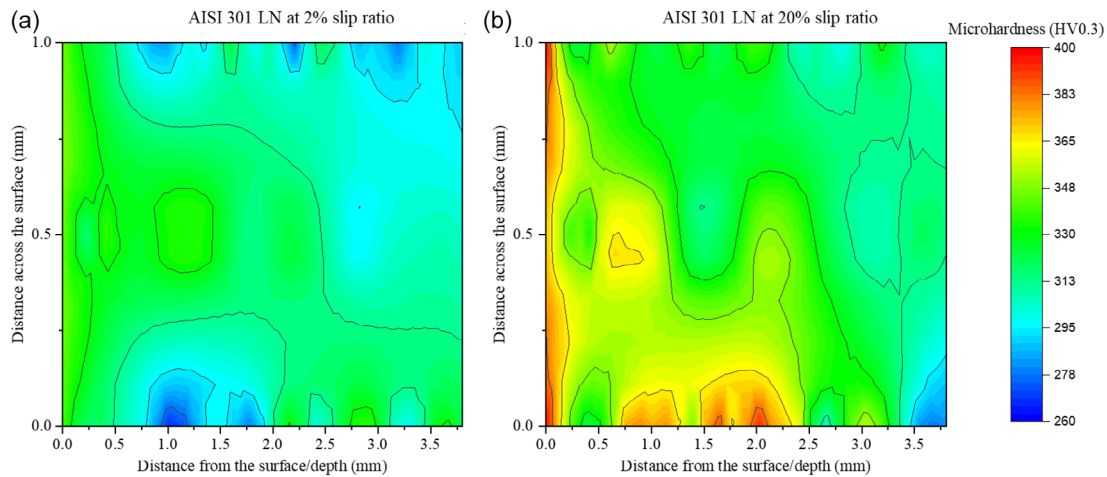


Figure 6. Vickers microhardness profiles (HV0.3) of AISI 301LN after run 2 at a) 2% and b) 20% slip ratios up to a depth of 3.8 mm from the contact surface.

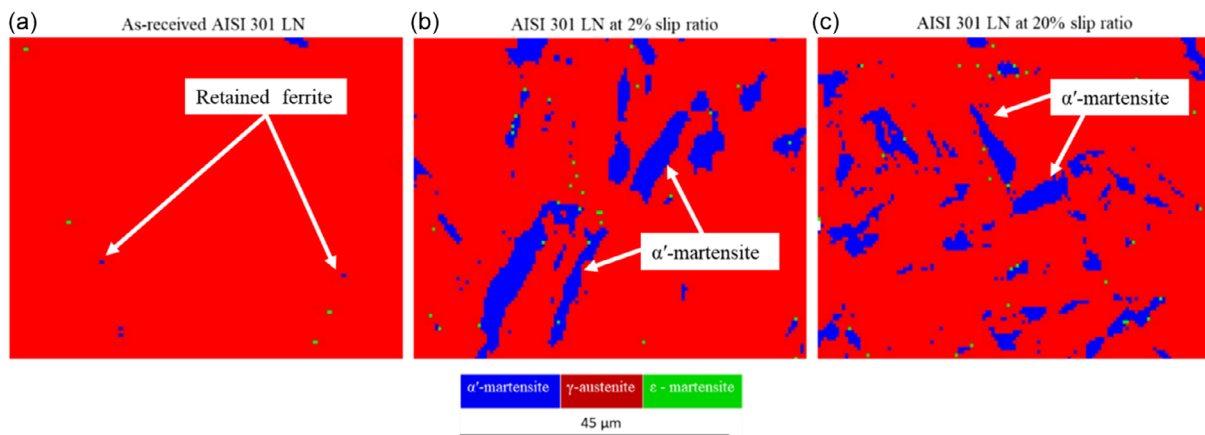


Figure 7. EBSD images of 301LN a) as-received close to the contact surface before test; b) after wear testing at 2%; and c) after wear testing at 20% slip ratio, showing induced martensite (α' -martensite) that has formed below the contact surface compared to the as-received specimen where only retained ferrite was only visible.

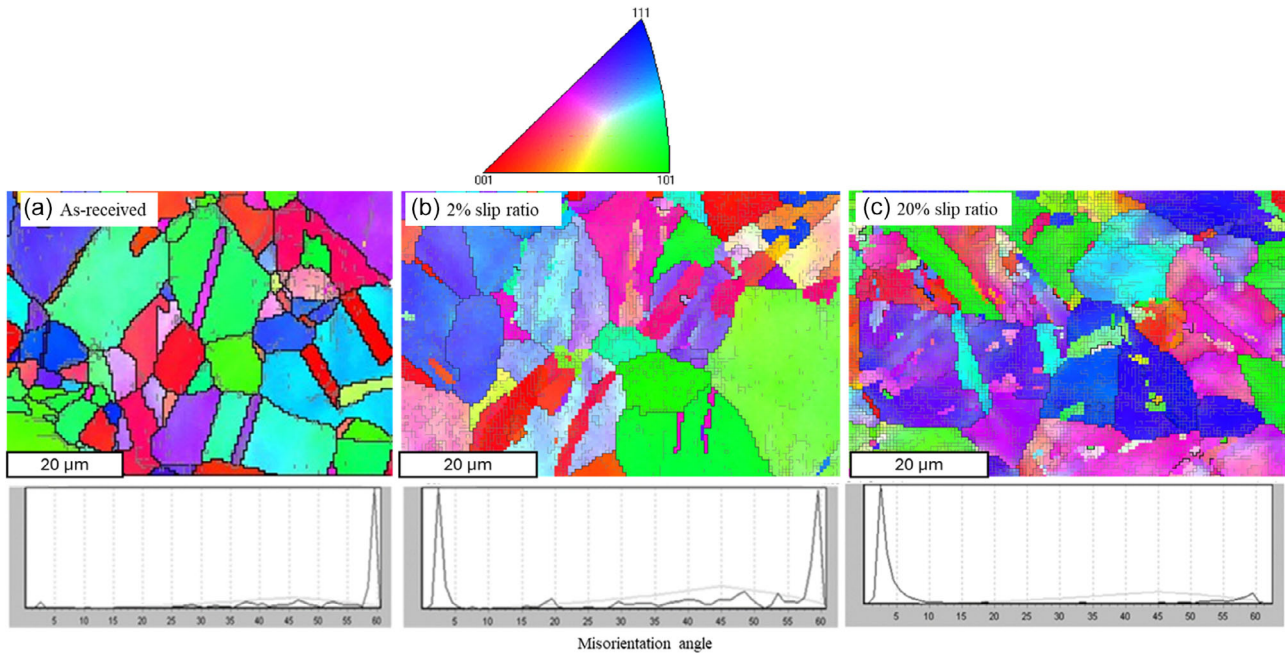


Figure 8. IPF maps of 301LN and corresponding misorientation plots in the x-direction at a step size of 0.5 μm ; a) as-received; b) after wear testing at 2%; and c) after wear testing at 20% slip ratios, both the grain rotation and low angle misorientation increased with an increase in the slip ratio due to increased plastic deformation.

primarily through twinning of the austenite rather than martensitic transformation. Additionally, higher amounts of twinning were observed at a 20% slip ratio compared to a 2% slip ratio, as illustrated in **Figure 9**. To accurately study the depth dependence of the formation of strain-induced martensite, XRD analysis was performed on two discs tested at 2% and 20% slip ratios on their contact surfaces and at 1 and 2 mm depths, **Figure 10** and **11**. As shown in Figure 10, there was significantly more strain-induced martensite at the contact surfaces of both 301LN discs with the 2% slip ratio disc having 87.8% of induced martensite whereas the 20% slip ratio had 85% compared to the martensite fractions at 1 and 2 mm depths from the contact

surface. The Ferritescope measurements (**Figure 5**) were lower than the XRD values because the Ferritescope is a volume (bulk) measurement technique and has a penetration depth ranging from 1 to 2 mm as stated in literature^[30–32] whereas the XRD analysis only measures at the surface with a few microns' penetration depth in steel specimens.^[33,34]

3.2. Effects of Slip Ratio on Wear Rate

During the first run (run 1), the wear rate was found to increase with the increase in slip ratio on both the AISI 301LN specimen and R350HT rail with a low rate of increase for the latter steel but

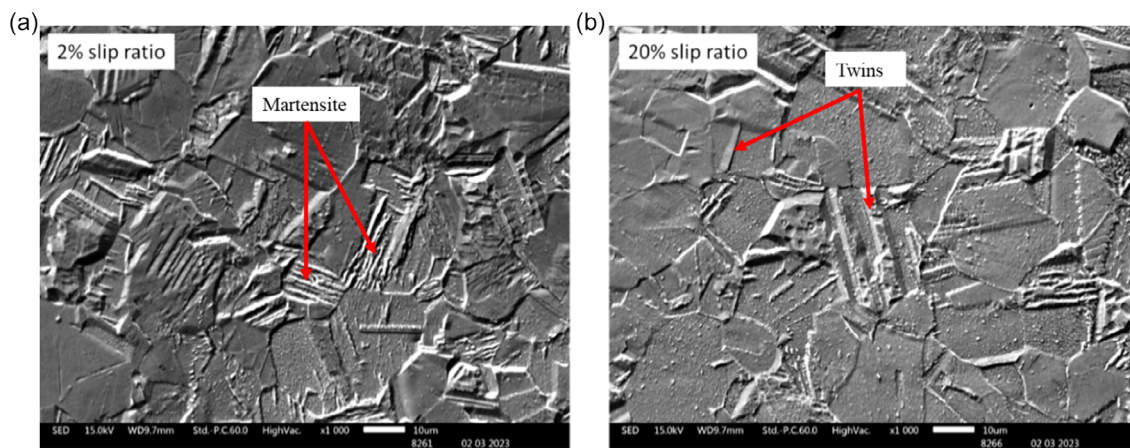


Figure 9. Micrographs of 301LN showing evidence of a) martensite formation at 2% slip ratio and b) formation twinning of austenite after run 2 at 20% slip ratio etched with aqua regia solution.

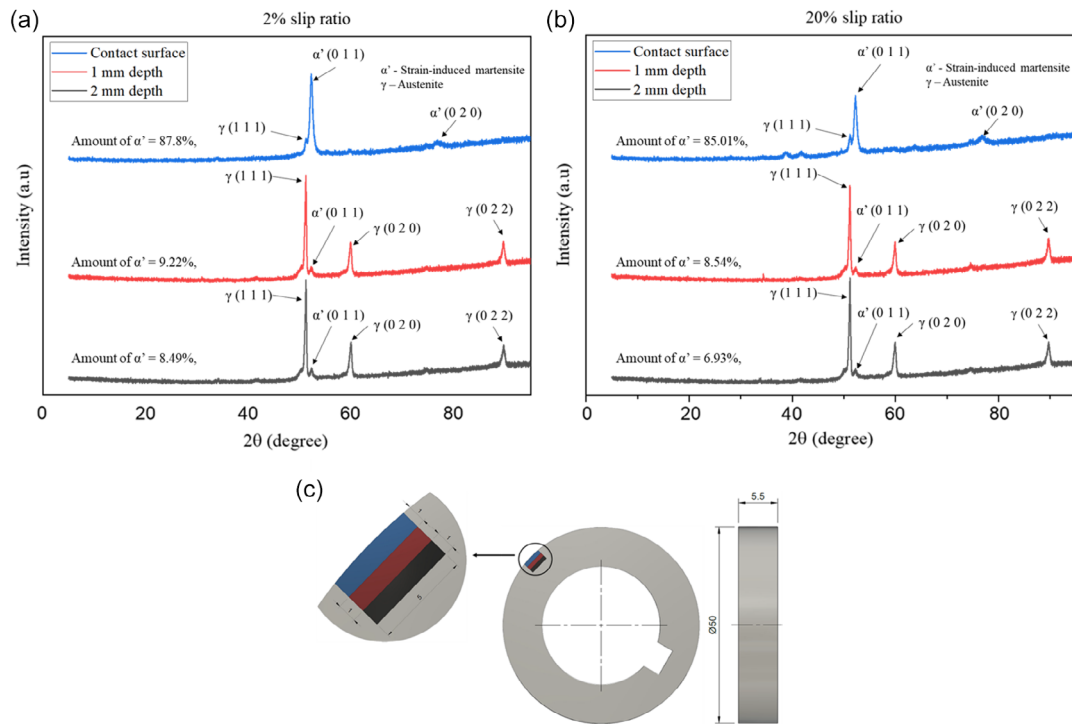


Figure 10. XRD patterns of worn 301LN specimen after run 2 at a) 2%; b) 20% slip ratios at different sampling positions showing the different peaks corresponding to induced martensite (α') and austenite (γ); and c) XRD sampling positions for the of AISI 301LN after wear testing at three different positions (contact surface, 1 and 2 mm depths).

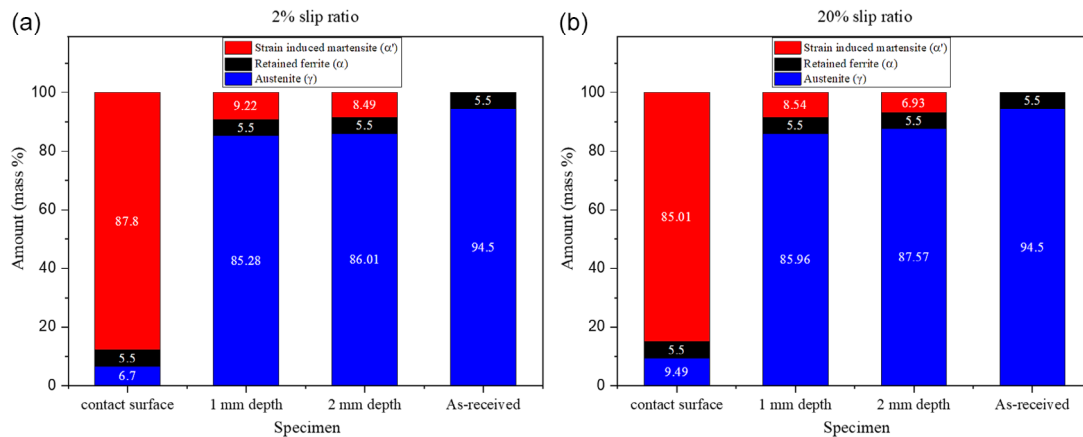


Figure 11. Localized amounts of strain-induced martensite (α' -martensite), austenite (γ), and retained ferrite (α) of the 301LN specimen at different sampling positions after run 2 a) 2% and b) 20% slip ratios compared to the as-received specimen which consisted of 5.5% of retained ferrite before test obtained using XRD analysis.

with a significant increase of wear rate ($511 \mu\text{g}/\text{mm}/\text{mm}^2$) for AISI 301LN at 20% slip ratio indicating catastrophic wear, **Figure 12**. The wear regimes (mild, severe, and catastrophic) were previously identified using a plot of wear rates and wear index in previous studies.^[35–37] When the same specimens were run again (run 2) under the same conditions but after surface cleaning and wear debris removal, lower wear rates were observed, and no catastrophic wear was observed. During the

second run, the AISI 301LN specimen showed a wear rate of $56 \mu\text{g}/\text{mm}/\text{mm}^2$ compared to $511 \mu\text{g}/\text{mm}/\text{mm}^2$ during the first run at 20% slip ratio. This was ascribed to the formation of martensite and twinning at the surface and subsurface resulting in an increase in surface hardness and brittleness.

The wear rate is influenced by the difference in hardness between the train wheel sample (AISI 301LN) and the R350HT rail steel sample. Initially, during the first run, the

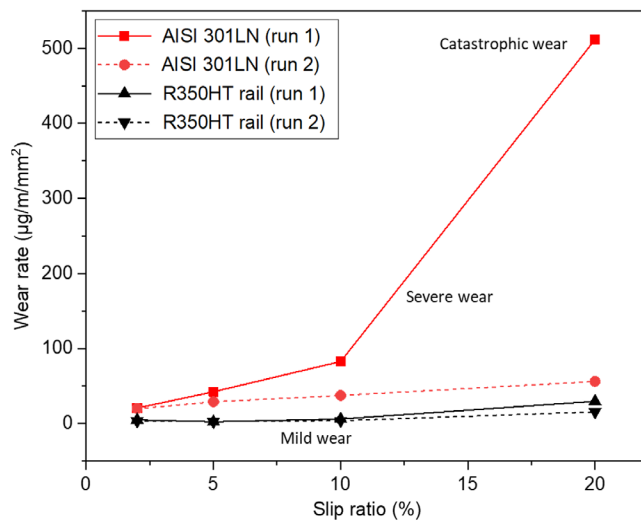


Figure 12. Wear rates versus slip ratio.

hardness of the train wheel sample was notably lower than that of the rail steel, leading to a high wear rate. However, the occurrence of martensitic transformation resulted in an increase in hardness. Consequently, during the second run, the disparity in hardness between the train wheel sample and the rail steel

was minimal, resulting in a significantly reduced wear rate. Unlike the first run samples, those from the second run had a significant amount of martensite and twinning formed from the initial runs. Increased spalling during the second run was encountered at a high slip ratio. This issue may be addressed through further investigation, potentially involving the inclusion of a tempering stage. This would be particularly relevant as the untempered martensite near the surface is inherently brittle and may require tempering to mitigate the problem of spalling (see **Figure 13**). The regions experiencing spalling coincide with areas where martensite formation was prominent. Spalling and high wear rates were inherent to the wear response during the first run (see Section 3.3), but not so during the second run, after reaching the saturation martensite percentage and removal of wear debris from the surfaces. Literature^[38–40] has shown that hardness plays a significant role in wear performance of steels, with harder steels performing better than softer ones. Compared with previous work on the same wear test rig by Leso et al.^[19] where the class B wheel steel was run against the R350HT rail steel under similar test conditions, the class B wheel performed better than the AISI 301LN even though AISI 301LN showed good work hardening ability. The formation of strain-induced martensite which is hard and brittle resulted in material loss by spalling hence the relatively higher wear rates observed for the MASS.

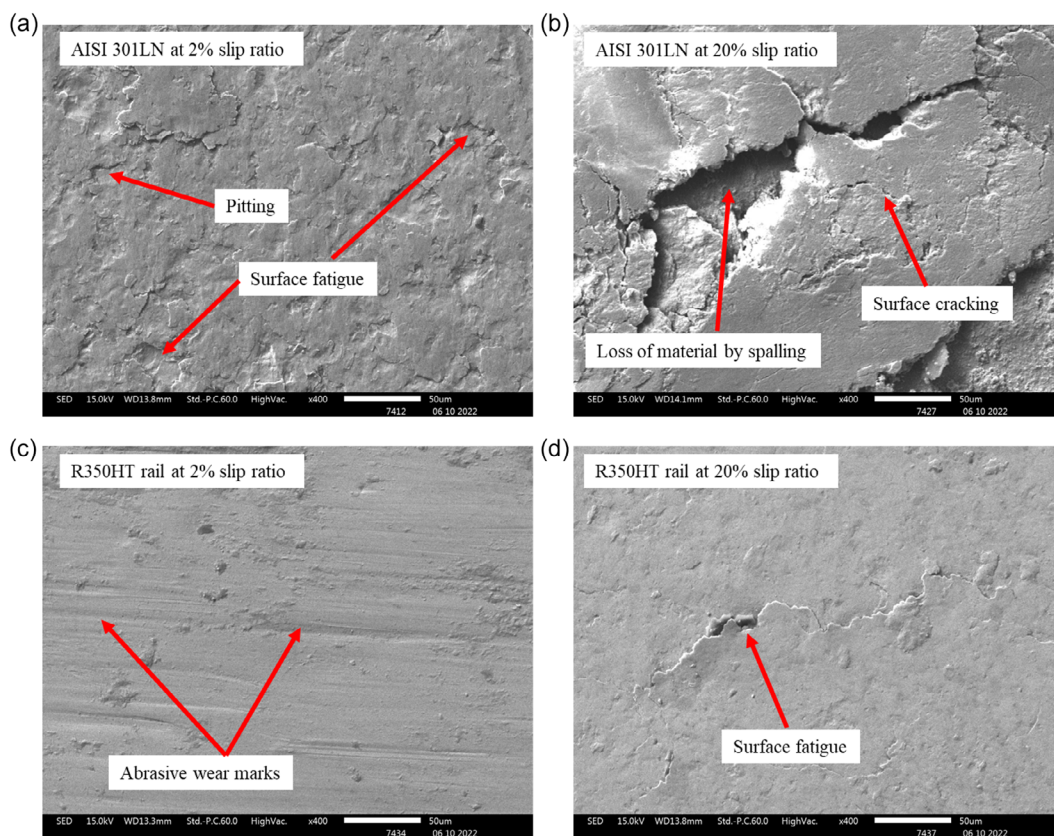


Figure 13. SEM micrographs of 301LN specimens at a) 2% and b) 20% slip ratio; and R350HT rail specimen at c) 2% and d) 20% slip ratio at showing the contact surface morphologies.

3.3. Surface Morphology

Figure 13 shows SEM micrographs of the contact surface after run 2. As may be seen, there was a high loss of material by spalling and intensive cracking at a slip ratio of 20% compared to 2%. The high amounts of bulk strain-induced martensite at all slip ratios make the surface hard and brittle facilitating crack initiation, propagation, and spalling. The presence of martensite and high slip ratios can significantly affect the material's fatigue behavior. Martensite tends to be harder and more brittle than the original material, making it more susceptible to fatigue crack initiation and propagation. The martensite that formed at the contact surfaces of 301LN discs is hard and brittle, which resulted in surface cracking causing material loss by spalling. Additionally, the transformation of austenite to martensite can induce residual stresses in the material, further contributing to fatigue damage. It is hypothesized that the reduction of material loss through spalling can be achieved by tempering the formed martensite, potentially leading to higher slip ratios without causing severe fatigue damage.

For the 301LN alloy investigated, the combined influence of the tensile strain percentage and the straining temperature on the fraction of martensite formed has earlier been quantified.^[1] This knowledge can be used to shed light on the surface and bulk strains of the wheels as a function of slip ratio. The bulk strains have accordingly been calculated using data from Figure 5 and similar. **Table 2** accordingly indicates that, at 20% slip ratio, the corresponding equivalent tensile strain was quite severe, at 39%. At the other end of the spectrum, at 2% slip ratio, the strain is significantly lower, at 16%. Using the local determinations of martensite fraction at various depths, using XRD (Figure 10), it becomes apparent that the subsurface strain distribution is highly variable. For example, these calculations applied to the 2% slip ratio case demonstrate that the surface strain is very high at 37% but that it rapidly drops off to 8% at 1 mm below the surface, **Table 3**. The higher spalling propensity and wear rates at the higher slip ratios must therefore be due to the very high surface strains characterized by high slip ratios, as shown in Table 2. To reduce the loss of material by spalling, a postwear test run 1 heat treatment (tempering) could be beneficial, improving the toughness of the materials and preventing surface cracking and spalling when the discs are rerun.

Table 2. Corresponding surface tensile strains and % cold working of 310 LN specimen at different slip ratios, based on the bulk Ferritescope readings and surface temperatures.

Slip ratio [%]	Maximum temperature recorded [°C]	Surface martensite measured by Ferritescope [%]	Corresponding tensile strain, from reference ^[1]
2	32.9	47.5	0.16
5	39.7	41.2	0.17
10	45.4	33.3	0.20
20	82.9	29.8	0.39

Table 3. Corresponding tensile strains and % cold working of 310 LN at different depths below the contact surface, tested at 2% slip ratio, based on localized XRD readings.

Depth below the contact surface	Maximum martensite measured by XRD [%]	Corresponding tensile strain, from ref. ^[1]
At the surface	93.3	0.370
1 mm below the surface	14.72	0.080
2 mm below the surface	13.99	0.077

4. Conclusion

The AISI 301LN MASS was found to have superior work hardening ability during rolling and sliding wear simulations compared to the eutectoid R30HT rail, due to the strain-induced martensite formation of the former steel. Wheels manufactured from the MASS demonstrated significantly increased hardness levels up to depth of 3.8 mm which should make it more suitable for rolling and sliding wear applications. Both Ferritescope and XRD analysis techniques confirmed the formation of strain-induced martensite at different contact conditions, with less martensite forming on the contact surface at high temperatures due to less driving force. However, during early stages of the wear testing, high wear rates were, however, observed for the AISI 301LN steel, with “catastrophic” wear being observed at high slip ratios. At later stages of the wear testing and after the removal of wear debris, wear rates decreased substantially but were still higher than that of the standard pearlitic wheel grade. The poor wear performance of the MASS was ascribed to a cracking and spalling mechanism that was introduced, especially at high slip ratios. The strain levels required for the martensite formation were calculated and it was demonstrated that very high surface strains, in the order of 0.37, were experienced by the 301LN wheels. The high surface strains are believed to have contributed to the cracking and spalling observed. For further work, after the first stages of wear, the worn 301LN discs could be tempered to soften the hard and brittle martensite which will improve toughness and could prevent further surface damage caused by material loss by spalling and cracking.

Acknowledgements

The authors would like to thank Columbus Stainless Steel (Pty) Ltd for supplying AISI 301LN materials and the University of Pretoria for providing research facilities. The authors would also like to thank Mr. Muhammed Salojee for helping with EBSD and Prof Johan de Villiers for helping with XRD data processing.

Conflict of Interest

The authors declare no conflict of interest.

Data Availability Statement

The data that support the findings of this study are available from the corresponding author upon reasonable request.

Keywords

metastable austenitic stainless steels, strengthening mechanism, wear and rolling contact fatigue, work-hardening rate

Received: February 13, 2024

Revised: May 15, 2024

Published online: June 25, 2024

-
- [1] T. W. Mukarati, R. J. Mostert, C. W. Siyasiya, *Mater. Sci. Eng. A* **2020**, 792, 1.
- [2] M. R. da Rocha, C. A. S. de Oliveira, *Mater. Sci. Eng. A* **2009**, 517, 281.
- [3] B. L. Ennis, E. Jimenez-Melero, E. H. Atzema, M. Krugla, M. A. Azeem, D. Rowley, D. Daisenberger, D. N. Hanlon, P. D. Lee, *Int. J. Plast.* **2017**, 88, 126.
- [4] Y. Hu, L. Zhou, H. H. Ding, G. X. Tang, R. Lewis, Q. Y. Liu, J. Guo, W. J. Wang, *Tribol. Int.* **2020**, 143, 1.
- [5] A. Shibata, H. Yonezawa, K. Yabuuchi, S. Morito, T. Furuwara, T. Maki, *Mater. Sci. Eng. A* **2006**, 438–440, 241.
- [6] C. L. Magee, R. G. Davies, *Acta Metall.* **1972**, 20, 1031.
- [7] R. Abbaschian, L. Abbaschian, R. E. Reed-Hil, in *Physical Metallurgy Principles*, 4th ed., Cengage Learning, Stamford **2010**.
- [8] M. Hauser, M. Wendler, A. Weiß, O. Volkova, J. Mola, *Adv. Eng. Mater.* **2019**, 21, 1800676.
- [9] T. W. Mukarati, R. J. Mostert, C. W. Siyasiya, *Steel Res. Int.* **2022**, 93, 2100459.
- [10] E. E. Magel, U.S. Department of Transportation, Federal Railroad Administration, Washington, DC **2011**.
- [11] K. Kanetani, T. Moronaga, *ISIJ Int.* **2021**, 61, 2629.
- [12] K. Kanetani, T. Mikami, K. Ushioda, *ISIJ Int.* **2020**, 60, 1774.
- [13] R. C. Dommarco, K. J. Kozaczek, P. C. Bastias, G. T. Hahn, C. A. Rubin, *Wear* **2004**, 257, 1081.
- [14] P. Haušild, V. Davydov, J. Drahošoupil, M. Landa, P. Pilvin, *Mater. Des.* **2010**, 31, 1821.
- [15] British Standards Institution, *Standard for Railway Applications. Track. Rail. Vignole Railway Rails 46 kg/m and Above*, BS EN 13674-1:2011, British Standards Institution, London **2011**.
- [16] J.-W. Seo, H.-K. Jun, S.-J. Kwon, D.-H. Lee, *Int. J. Fatigue* **2016**, 83, 184.
- [17] L. Deters, M. Proksch, *Wear* **2005**, 258, 981.
- [18] R. Lewis, E. Magel, W.-J. Wang, U. Olofsson, S. Lewis, T. Slatter, A. Beagles, *Proc. Inst. Mech. Eng. F J. Rail Rapid Transit* **2017**, 231, 760.
- [19] T. P. Leso, C. W. Siyasiya, R. J. Mostert, J. Moema, *Tribol. Int.* **2022**, 174, 1.
- [20] D. Fletcher, J. Beynon, *J. Test. Eval.* **2000**, 28, 267.
- [21] Y. Hu, W. J. Wang, M. Watson, K. Six, H. Al-Maliki, A. Meierhofer, R. Lewis, *Wear* **2023**, 512–513, 204528.
- [22] W. J. Wang, S. R. Lewis, R. Lweis, A. Beagles, C. G. He, Q. Y. Liu, *Wear* **2017**, 376–377, 1892.
- [23] Q. Lian, G. Deng, A. K. Tieu, H. Li, Z. Liu, X. Wang, H. Zhu, *Tribol. Int.* **2020**, 141, 105943.
- [24] A. Ward, R. Lewis, R. S. Dwyer-Joyce, *Tribol. Ser.* **2003**, 41, 367.
- [25] P. J. Bolton, P. Clayton, *Wear* **1984**, 93, 145.
- [26] S. Timoshenko, J. N. Goodier, in *Theory of Elasticity*, 2nd ed., McGraw-Hill, New York, NY **1951**.
- [27] R. G. Budynas, J. K. Nisbett, in *Shigley's Mechanical Engineering Design*, 9th ed., McGraw-Hill, New York, NY **2011**.
- [28] J. Talonen, P. Aspegren, H. Hänninen, *Mater. Sci. Technol.* **2004**, 20, 1506.
- [29] J. Talonen, H. Hänninen, P. Nenonen, G. Pape, *Metall. Mater. Trans. A* **2005**, 36, 421.
- [30] V. Kaňa, V. Pernica, A. Zadera, V. Krutiš, *Arch. Foundry Eng.* **2019**, 2, 85.
- [31] L. G. Ionescu, M. V. Pantawane, C. Tanase, R. V. Sichim, C. A. Dascalu, B. Ghibansa, *Crystals* **2023**, 13, 1173.
- [32] R. Kshirsagar, S. Jones, J. Lawrence, J. Tabor, *J. Mater. Process. Technol.* **2019**, 274, 116278.
- [33] P. Rozenak, E. Shani, *Metall. Mater. Trans. A* **2012**, 43, 4028.
- [34] J. R. Tolchard, A. Sømme, K. J. Solberg, K. G. Solheim, *Mater. Charact.* **2015**, 99, 238.
- [35] R. Lewis, R. S. Dwyer-Joyce, U. Olofsson, J. Pombo, J. Ambrósio, M. Pereira, C. Ariaudo, N. Kuka, *Proc. Inst. Mech. Eng. F J. Rail Rapid Transit* **2010**, 224, 125.
- [36] L. Ma, C. G. He, X. J. Zhao, J. Guo, Y. Zhu, W. J. Wang, Q. Y. Liu, X. S. Jin, *Wear* **2016**, 366–367, 13.
- [37] W. J. Wang, R. Lewis, B. Yang, L. C. Guo, Q. Y. Liu, M. H. Zhu, *Wear* **2016**, 362–363, 146.
- [38] R. Stock, R. Phippan, *Wear* **2011**, 271, 125.
- [39] P. Clayton, D. Danks, *Wear* **1990**, 135, 369.
- [40] M. Sato, P. M. Anderson, D. A. Rigney, *Wear* **1993**, 162–164, 159.